JOURNAL OF THERMOPHYSICS AND HEAT TRANSFER
Vol. 8, No. 1, Jan.–March 1994

Review of Numerical Procedures for Computational Surface Thermochemistry

Frank S. Milos* and Daniel J. Rasky†
NASA Ames Research Center, Moffett Field, California 94035

Models and equations for surface thermochemistry and near-surface thermophysics of aerodynamically heated thermal protection materials are reviewed, with particular emphasis on computational boundary conditions for surface mass and energy transfer. The surface energy and mass balances, coupled with an appropriate ablation or surface catalysis model, provide complete thermochemical boundary conditions for a true multidisciplinary solution of the fully coupled fluid-dynamics/solid mechanics problem. Practical approximate solutions can be obtained by using a detailed model with full thermophysics for either the solid or fluid phase and a semianalytic method for the other half of the problem. A significant increase in the state-of-the-art in aerothermal computational fluid dynamics is possible by uniting computational fluid dynamic (CFD) methodology with surface thermochemistry boundary conditions and the heat-balance-integral method.

Nomenclature

A_i = area in direction i, m^2
a = partial density coefficient, kg/m^3
B = pre-exponential constant, 1/s
B' = dimensionless mass flux at surface
b = exponent in heat-balance integral model
$C_f/2$ = skin friction coefficient
C_h, C_m = Stanton numbers for heat, mass transfer
c_p = heat capacity, J/kg-K
c_1 = drag coefficient, 1/m^2
c_2 = drag coefficient, 1/m
D = diffusion coefficient, m^2/s
E = activation temperature, K
F = radiation view factor
$\mathcal{F}$ = general ablation function
$\mathcal{G}$, $\mathcal{H}$ = boundary-layer shape factors
h = enthalpy, J/kg
h_r = recovery enthalpy, J/kg
h' = total enthalpy, J/kg
I, J = influence coefficients for C_h, C_f
k = thermal conductivity, W/m-K
M = molecular weight, kg/mole
$\dot{m}$ = mass flux, kg/m^2-s
N_c = number of species
N_d = number of decomposition reactions
N_{el} = number of elements
N_r = number of surface reactions
$\boldsymbol{n}$ = outward unit normal vector
P = pressure, kg/m-s^2
Q^* = ablation model constant, J/kg
q = heat flux, W/m^2
q_{cond} = conduction heat flux, W/m^2
q_r = radiative heat flux, W/m^2
R = gas constant, kg-m^2/mole-K-s^2
$\mathcal{R}$ = recovery factor
r_b = body radius, m
r_k = net rate for surface reaction k, mole/m^2-s
r_{shock} = shock radius, m
s = stream length, m
$\dot{s}$ = recession rate, m/s
T = temperature, K
T_{abl} = minimum ablation temperature, K
T_{init} = initial temperature, K
t = time, s
u = streamwise velocity, m/s
V = numerical cell volume, m^3
$\boldsymbol{V}$ = superficial gas velocity vector, m/s
x = inward normal coordinate, m
Y = ablation gas mass ratio, kg/kg thermal protection system material
y = species mass fraction
$\bar{y}$ = elemental mass fraction
z = moving inward coordinate, m
ϵ = emissivity
α = absorptivity
γ = recombination rate coefficient
δ = boundary-layer thickness, m
δ_T = heat-balance integral thermal layer thickness, m
δ^* = displacement thickness, m
ε = void fraction
η = outward normal coordinate, m
θ = momentum thickness, m
λ = blowing correction parameter
μ = viscosity, kg/m-s
ν = stoichiometric coefficient
ξ = heat-balance integral dependent variable, J/m^3
ρ = density, kg/m^3
φ = dimensionless density
σ = Stefan-Boltzmann constant, W/m^2-K^4
ϕ = energy thickness, m
ψ = decomposition reaction order

Subscripts
c = char
e = boundary-layer edge
f = fail
g = pyrolysis gas
i = normal shock edge
N = nitrogen
O = oxygen
s = solid or surface

Presented as Paper 92-2944 at the AIAA 27th Thermophysics Conference, Nashville, TN, July 6–8, 1992; received July 22, 1992; revision received Jan. 20, 1993; accepted for publication Feb. 4, 1993.

*Aerospace Engineer, Thermal Protection Materials Branch. Member AIAA.
†Chief, Thermal Protection Materials Branch. Member AIAA.

T = translational
V = vibrational
w = wall
∞ = freestream

I. Introduction

COMPUTATIONAL fluid dynamics (CFD) and computational solid mechanics (CSM) codes typically treat fluid/solid surface boundary conditions in a very simplified or idealized manner such as a constant prescribed temperature or heat flux and with zero mass transfer. However, in energetic hypersonic environments, thermal protection system (TPS) materials interact with the flow through diverse thermochemical and thermophysical mechanisms including ablation, shape change, pyrolysis, melt flow, and spallation. Even in the nonablating case, real materials conduct heat, catalyze reactions, and participate in radiative energy exchange.

Computational surface thermochemistry (CST) is a multidisciplinary activity to bridge the gap between existing CFD and CSM methodologies. The objective of the CST program at NASA Ames is to develop new multidimensional, near-surface, material/fluid interaction codes which will interface between existing CFD and CSM codes and which will provide detailed modeling of these surface and near-surface thermochemical phenomena.

The specific application of this work is the design and analysis of thermal protection systems for three-dimensional hypersonic vehicles and spacecraft at angle of attack. Solution of this problem involves transient CSM analyses of the material thermophysics, a sequence of steady-state CFD analyses to determine the time-history of the aerothermal heating, and strongly coupled CST boundary conditions.

This problem is of critical importance for optimization of the TPS for future hypersonic vehicles and spacecraft. Thermal protection systems are traditionally designed with one- and two-dimensional engineering codes. Occasionally, a detailed computational solution is obtained, but these solutions rarely contain the correct CST boundary conditions. To compensate for uncertainties in the analyses, a safety margin of extra TPS material is added to the final design, and the structural weight must also be increased.

The TPS/structural weight is typically significantly larger than the payload weight, by up to a factor of four for planetary probes.[1] Therefore, a reduction in the TPS weight has a cascade effect: the structural weight is also reduced, resulting in a direct increase in payload and scientific capability. Clearly there is a need for more accurate, multidimensional computational tools which can be used to reduce the uncertainties in TPS analysis and to optimize the TPS distribution around hypersonic vehicles and spacecraft.

A review of the work in the areas of thermophysics and advanced numerical methods reveals four parallel and relatively independent efforts each focused on specific aspects of the overall problem under consideration here. They are as follows:

1) CFD technology continues to develop in the areas of nonequilibrium flow, multispecies kinetics and transport properties, radiation transport, and three-dimensional capabilities. However, most codes use primitive surface boundary conditions and cannot realistically be used for TPS design. CFD calculations have not yet taken into account spatially varying surface temperature and heat flux, a realistic surface energy balance, thermal soak into the TPS material, and thermochemical ablation modeling. The computational expense of advanced CFD methods limits their utility for trajectory-based analysis.

2) Research at the Aerotherm Corporation (formerly Acurex) has focused on near-surface thermophysics,[2-4] ablation models,[5-7] and the coupling of genuine CST boundary conditions with numerical methods.[3,4,8,9] A number of extremely useful engineering codes have been developed[10-12] which utilize semianalytic numerical methods for at least one-half of the physical problem. However, to date, these models have not been coupled with modern CFD and CSM numerical procedures.

3) Researchers at the NASA Ames Research Center[13-16] have studied in detail aerothermal heating predictions for the nonablating case. They have determined catalytic coefficients, demonstrated the importance of surface catalysis, nonequilibrium kinetics, and multispecies transport properties for the prediction of aerothermal heating, and recently incorporated a surface energy balance with surface catalytic reactions into a state-of-the-art CFD code.

4) Computational solid mechanics has advanced to the point where highly detailed thermal conduction, linear deformation, stress, and failure analyses can be made quickly with personal computer-based software.[17] This finite element technology could conceivably be applied to material thermophysics if the effort was made to develop "thermophysics elements" and "surface thermochemical elements."

Review of these parallel efforts shows that the models for surface thermochemistry and near-surface thermophysics are already in an advanced state of development, but have been either neglected or not well-understood by the CFD and CSM communities. Significant progress in the development of useful numerical tools is possible if these parallel efforts could be united.

To encourage this progress, in this work we review and publicize the existing models for TPS thermophysics, list in detail the surface energy and mass balances that should be used for true multidisciplinary CFD and CSM solutions, highlight the approximate methods that provide missing pieces of the surface energy balance, and outline our approach and recommendations for solution of this problem.

II. Near-Surface Thermochemical Models

This section reviews the thermochemical models, equations, and other relevant phenomena for the analysis of surface thermochemistry and of near-surface thermophysics in both the gas and solid phases. Computational methods for nonablating TPS systems are considered first, followed by ablating TPS systems, pyrolyzing TPS systems, and CFD methods for ablation.

A. CFD Analyses for Nonablating TPS Systems

Nonablating thermal protection systems are used on reusable hypersonic vehicles, on the leeward portions of hypersonic vehicles, and in low-pressure (high-altitude) environments where the heating rate or the duration of heating are insufficient to cause significant amounts of vaporization or melt flow of the surface material.

Boundary-layer,[15] shock-layer,[18] parabolized Navier-Stokes (PNS),[19,20] and full Navier-Stokes (NS)[16] codes all recently have been employed to predict the aerothermal loads on nonablating surfaces. These studies indicate that chemical nonequilibrium, species diffusion, surface catalysis, the surface energy balance (SEB), thermal nonequilibrium, and uncertainties in reaction kinetics and transport coefficients are all important considerations in the analysis.

Kinetic rate coefficients have been tabulated for a two-temperature T-T_V model.[21,22] Self-consistent transport coefficients for multicomponent mixtures can be obtained using the model of Bartlett et al.[23] Alternatively, Wilke[24] mixing rules are often used with Blottner's species-viscosity curve fits,[25] Eucken's relation for the Prandtl number,[26] Lee's binary diffusion coefficients,[27] and/or some assumptions of constant Prandtl, Schmidt, and Lewis numbers.

The nonablating surface actively participates in energy exchange with the flow and as a site for heterogeneous chemical reactions. A general form of the SEB for a nonequi-

librium CFD solution, which serves as a thermal boundary condition, is

$$q_w^{\mathrm{CFD}} = k_T \frac{\partial T}{\partial \eta} + k_V \frac{\partial T_V}{\partial \eta} + \sum_{i=1}^{N_c} \rho h_i D \frac{\partial y_i}{\partial \eta} + q_r \qquad (1a)$$

$$= (1 - \alpha_{sw}) q_r + F\sigma \epsilon_{sw} T_w^4 + q_{\mathrm{cond}} \qquad (1b)$$

where η is the outward surface-normal direction. In Eq. (1) the terms on the right side account for heat conduction to the surface by translational and vibrational modes, respectively, the diffusive chemical energy flux to the surface, the radiative flux to the surface, the reflected radiation, the reradiation from the surface, and the heat conduction into the solid. The surface is assumed to have zero transmissivity. The surface emissivity ϵ_{sw} and absorptivity α_{sw} are material-dependent and can be functions of temperature. Correlations are available for estimation of q_r at the stagnation point.[28] However, the calculation of q_r is not straightforward owing to radiation absorption in the boundary or shock layer. The total aerothermal heat flux to the surface, q_w^{CFD}, is a time- and location-dependent quantity to be determined by the CFD calculation for the purpose of TPS design. The commonly used "CFD adiabatic wall" boundary condition, $q_w^{\mathrm{CFD}} = 0$, while being numerically convenient, has no realistic physical meaning and is inappropriate for aerothermal analysis.

The conduction term q_{cond} is indeterminate from the CFD analyses, unless a numerical or semianalytic CSM solution is also computed (cf. Sec. III). A "radiative equilibrium" energy balance (REEB) solution is obtained by setting $q_{\mathrm{cond}} = 0$ while retaining all the other terms in Eq. (1). However, this rarely is a reasonable assumption for a nonablating surface. It is obvious that T_w is a function of both time and location on the surface. The computationally-simple boundary condition $T \equiv T_w$ is not warranted in aerothermal analysis except for cold wall computations or for actively cooled structures.

The chemical energy flux term is zero only if the surface is completely noncatalytic. However, all TPS materials catalyze to some extent the recombination of gas-phase atomic species. Three reactions of interest for air environments are

$$\begin{aligned} \mathrm{N} + \mathrm{N} &\rightarrow \mathrm{N}_2 + \Delta h_1 \\ \mathrm{O} + \mathrm{O} &\rightarrow \mathrm{O}_2 + \Delta h_2 \\ \mathrm{N} + \mathrm{O} &\rightarrow \mathrm{NO} + \Delta h_3 \end{aligned} \qquad (2)$$

where the Δh are positive heats of recombination.

Mass conservation requires that a specie's diffusion rate to the surface equals its net rate of disappearance by surface reactions

$$\rho D \frac{\partial y_i}{\partial \eta} = \sum_{k=1}^{N_r} \nu_{ki} r_k M_i, \qquad i = 1, N_c \qquad (3)$$

where r_k are the net forward reaction rates and ν_{ki} are the stoichiometric coefficients of the reactions (positive for reactants). Equation (3) is the surface mass balance (SMB) for the nonablating case. Note that the chemical energy flux term in Eq. (1a) equals $\Sigma\, r_k \Delta h_k$ as required to account for the energy production or loss owing to surface reactions.

Hypersonic shock and boundary layers, particularly those at low pressures, often contain a nonequilibrium excess of atomic oxygen and nitrogen. When the nonequilibrium flow contacts a catalytic surface, reactions [Eq. (2)] move in the forward direction and heat is generated at the surface. Consequently, the thermal load increases with catalytic efficiency, and a fully catalytic surface experiences the highest heat flux. This catalytic-heating effect has been demonstrated by space shuttle heat-transfer data.[29] Therefore, unless a hypersonic flow is at sufficiently high pressure to be in chemical equilibrium, or unless the surface is completely noncatalytic, surface catalysis effects should be taken into account to predict the aerothermal heating.

Catalytic reactions generally consist of several substeps which may include adsorption of atomic species onto the surface, reactions between adsorbed species or between adsorbed species and gas-phase atoms, and desorption of the molecular product from the surface. The overall reaction rate r_k can take several analytic forms, depending on which substep is rate controlling, and contains several pressure and temperature-dependent coefficients.[30] The Eley-Rideal mechanism[31,32] suggests that the reactions are likely to be first-order at low temperatures and second-order at high temperatures.

During the past several years, a phenomenological rate model for surface catalysis has been developed by Stewart and coworkers.[13-16] In this model, the surface reaction rates are written as first order in density

$$\begin{aligned} r_1 &= \frac{\gamma_N \rho_N}{M_N} \sqrt{\frac{RT_w}{2\pi M_N}} \\ r_2 &= \frac{\gamma_O \rho_O}{M_O} \sqrt{\frac{RT_w}{2\pi M_O}} \\ r_3 &\ll r_1, r_2 \end{aligned} \qquad (4)$$

Temperature variations of the recombination coefficients γ_N and γ_O that are consistent with the above rate expressions have been obtained from experimental data from arcjet and flow-reactor tests for reaction cured glass.[16] A pressure-dependent decrease in γ at high temperature is attributed to the change from first-order to second-order kinetics.[33]

B. Thermophysics of Noncharring TPS Materials

In a hypersonic heating environment, noncharring TPS materials, such as carbon-carbon and silica, lose mass only by ablation and melt/fail mechanisms. Detailed analysis of the performance of such TPS materials must consider the in-depth energy equation, the surface and thermal property variations with temperature, the SMB and SEB, and ablation modeling.

Surface and thermal property data have been tabulated[34] for a variety of TPS materials and are being incorporated into a material data base program.[35] Relevant data are the surface emissivity and absorptivity, the heats of formation and ablation, the density and thermal expansion coefficient, and the thermal conductivity and heat capacity.

For noncharring TPS materials, several ablation models are available with varying degrees of sophistication. The least-general ablation model is an $\dot{s}$ vs T_w model which specifies the recession rate as a function of surface temperature. This empirical model relies on experimental data for ablation in the pressure range of interest. The $\dot{s}$ vs T_w model is used for certain polymeric materials which ablate from the surface in a manner that currently cannot be well-predicted by chemical equilibrium or kinetic models.[36,37]

The Q^* model is the most common engineering-level model for ablation. In this model, Q^* is the effective heat of ablation

$$\dot{m}_{sw} = \dot{s}\rho_{sw} = q_w / Q^*, \qquad \text{for} \qquad T_w \geq T_{\mathrm{abl}}$$

where $\dot{m}_{sw}$ is the ablation mass flux and q_w is the net aerothermal heat flux. The Q^* model is most useful for high-heating conditions and for low-conductivity materials where steady-state recession is a good approximation. This model cannot predict accurately the surface temperature history and heat soak for a TPS material.

Thermochemical ablation is the most general and widely applicable TPS ablation model. This model[2,38] was developed at the Aerotherm Corporation and is programmed into two computer codes: 1) aerotherm chemical equilibrium (ACE),[5] and 2) general nonequilibrium ablation thermochemistry (GNAT).[6] Thermochemical ablation models are obtained from

a solution of the equations for thermodynamic equilibrium or nonequilibrium between the TPS material and the atmosphere of interest, coupled with surface mass and energy balances and (typically) boundary-layer transfer coefficients. The net result of the calculations is a set of thermochemical tables relating surface temperature and pressure to the dimensionless surface mass fluxes owing to ablation and to mechanical fail. These tables numerically represent a general ablation function $\mathcal{F}(T, P, B'_s, B'_f) = 0$ for a specific TPS material, such as carbon, and a specific boundary-layer-edge gas, such as air. Reference 38 contains complete details of the procedure.

In the thermochemical tables, the surface mass fluxes are nondimensionalized with the mass transfer coefficient to define the dimensionless variables $B'_s = \dot{m}_{sw}/\rho_e u_e C_m$ and $B'_f = \dot{m}_{fw}/\rho_e u_e C_m$. The shape of the B' curves depends on the material composition, the choice of allowable surface and gas-phase species, the atmospheric composition, and whether or not kinetically limited reactions or fail modes occur. Experience, insight, and experimental data are all important ingredients in the development of accurate thermochemical tables for a selected TPS material. However, once such tables have been generated, they are applicable over a wide range of aerothermal heating conditions.

Figure 1 shows $B'_s(T, P)$ for pure thermochemical ablation of carbon in air.[5] As the pressure is increased, a higher surface temperature is needed to reach the same dimensionless ablation rate. For any pressure, at the highest ablation rates, carbon sublimation is the primary mass loss mechanism, and $C_3(g)$ is the predominant ablative species. However, below $B' \approx 0.2$, surface oxidation reactions dominate, and CO is the major species leaving the surface.

Thermochemical surface equilibrium overestimates the carbon ablation rate at low temperatures and pressures. To obtain less-conservative ablation predictions it is appropriate to treat heterogeneous oxidation of carbon with kinetic rate-

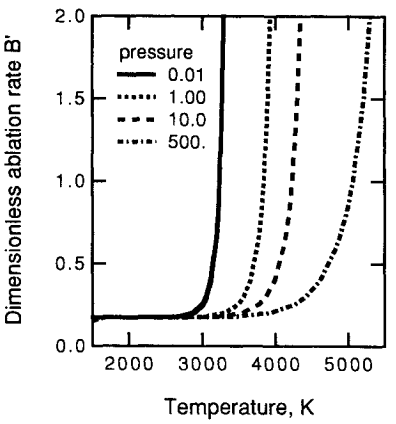

Fig. 1 Dimensionless ablation rate for carbon. Full equilibrium surface thermochemistry; pressure in atm.

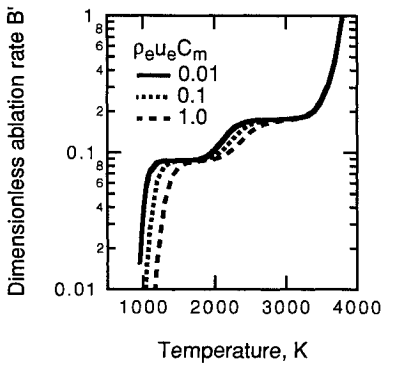

Fig. 2 Dimensionless ablation rate for carbon. Thermochemical solution with surface kinetics; P = 1 atm and $\rho_e u_e C_m$ in lbm/ft²-s.

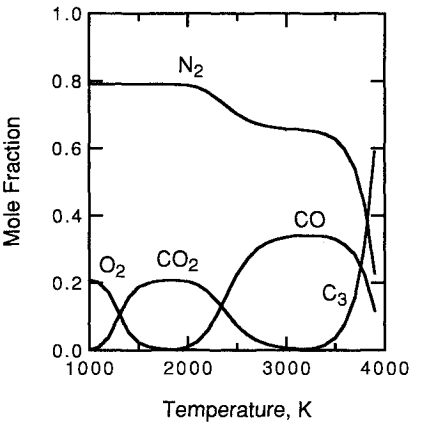

Fig. 3 Surface chemical species for carbon ablation. Thermochemical solution with surface kinetics; P = 1 atm and $\rho_e u_e C_m$ = 1 lbm/ft²-s.

limited reactions. Thermochemical tables were created[5] using kinetics derived from Ref. 39 for the reaction $2C(s) + O_2 \rightarrow 2CO$. Results for one pressure and three mass transfer coefficients are shown in Fig. 2. For each curve, the lowest plateau at $B' \approx 0.09$ is a result of kinetic production of CO followed by fast oxidation to CO_2 at the surface. The higher plateau is caused by diffusion-limited production of CO. Figure 3 shows the predicted gas-phase mole fractions at the surface. C_3 is the major ablative species only at highest temperatures and ablation rates.

For an ablating surface, the SMB takes different forms depending on whether or not the flow is in chemical equilibrium. For equilibrium flow, it is convenient to utilize elemental mass fractions $\tilde{y}$ which are known for the TPS material and which are variables in the CFD solution. In this case, the SMB is

$$\rho D \frac{\partial \tilde{y}_k}{\partial \eta} = \dot{m}_{sw}(\tilde{y}_k - \tilde{y}_{swk}), \qquad k = 1, N_{el} \tag{5a}$$

where the $\tilde{y}_{sw}$ are elemental mass fractions in the nonfailing portion of the TPS material. Alternatively, for a nonequilibrium flow, it is preferable to specify species fluxes at the surface. The SMB can be written

$$\rho D \frac{\partial y_i}{\partial \eta} = \sum_{k=1}^{N_r} \nu_{ki} r_k M_i + \dot{m}_{sw}(y_i - Y_{swi}), \qquad i = 1, N_c \tag{5b}$$

where Y_{swi} is the mass of species i produced in the ablation gas per mass of TPS material ablated. The Y_{sw} are positive for ablation products, negative for atmospheric species which are consumed in the ablation process, and sum to unity. The effective heat of ablation is $\Sigma\, h_i Y_{swi} - h_{sw}$.

The SEB contains only one additional term to account for ablation

$$q_w^{CFD} = (1 - \alpha_{sw})q_r + F\sigma\epsilon_{sw}T_w^4 + q_{cond} + \dot{m}_{sw}(h_w - h_{sw}) \tag{6}$$

where q_w^{CFD} is defined by Eq. (1a) and h_w is the enthalpy of the gas phase at the surface.

The aerothermal heat flux is often approximated using transfer coefficient methodology. This technique is particularly useful when coupled with thermochemical ablation tables. A commonly used approximation,[37] which assumes equal species diffusion coefficients and $C_m = C_h$, is

$$q_w^{CFD} \approx \rho_e u_e C_h(h_r - h_w) + q_r \tag{7}$$

The wall-gas enthalpy h_w is a dependent variable in thermochemical ablation tables. The blown Stanton number C_h can

be related to the unblown value C_{h0} by the "blowing correction" approximation

$$\frac{C_h}{C_{h0}} = \frac{2\lambda B'_s}{e^{2\lambda B'_s} - 1} \tag{8}$$

which is derived from boundary-layer film theory. This expression can be inaccurate at very high blowing rates or small Prandtl numbers. The classical value[40] of λ is 0.5, but the authors have used values ranging from 0.3 to 1.3 in different circumstances.

For low-conductivity materials or at high ablation rate, the conduction flux is approximately equal to the steady-state value:

$$q_{\text{cond}}^{\text{SSEB}} = \dot{m}_{sw}h_{sw} + \dot{m}_{fw}h_{fw} - [\dot{m}_{sw} + \dot{m}_{fw}](h_s)_{\text{in depth}} \tag{9}$$

The steady-state surface energy balance (SSEB) is obtained by substitution of Eq. (9) into the SEB, Eq. (6). The "radiative equilibrium" energy balance (REEB) uses $q_{\text{cond}} = 0$ in the SEB. This assumption is worse than using the SSEB, because the conduction heat flux is, in general, larger than the SSEB value.

C. Thermophysics of Charring TPS Materials

When heated, many TPS materials, including phenolics and plastic resins, experience a series of chemical reactions that release gaseous by-products. Upon completion of these reactions, the porous residual char that remains has lower density than the original "virgin" solid and different thermal and structural properties. Chars generally have low mechanical strength and spall at high heating conditions. However, exceptions to this rule are structural ceramic ablators which contain a rigid noncharring porous matrix in addition to the pyrolyzing resin.[41] Detailed analysis of charring TPS materials must consider the in-depth energy and mass-decomposition equations, the porosity, surface, and thermal properties as functions of density (or char fraction) as well as temperature, the additional terms in the surface balances and ablation models, and the flow of the pyrolysis gas.

Charring materials are modeled as a sum of constituents, each of which independently decomposes according to an Arrhenius-type reaction rate expression.[3,42] The decomposition equations can be written

$$\rho_s = \rho_c + \sum_{i=1}^{N_d} a_i\varphi_i \tag{10a}$$

$$\frac{d\varphi_i}{dt} = -B_i e^{-E_i/T}\varphi_i^{\psi_i} \qquad i = 1, N_d \tag{10b}$$

where ρ_c is the char density, φ_i are dimensionless constituent densities, and N_d is the number of decomposition reactions (typically 2 or 3). The decomposition parameters a, B, E, and ψ have been tabulated for a variety of charring TPS materials.[34]

The solid density is a function of both location and time, owing to the time history of the thermal field. To determine the density history of a charring material, Eqs. (10) must be solved concurrently with an energy conservation equation

$$V\frac{\partial}{\partial t}[\rho_s h_s + \varepsilon\rho_g h_g] = -\sum_i A_i(k_s\nabla T)\cdot\boldsymbol{n} + (h_g - h_s)V\frac{\partial\rho_s}{\partial t} - \sum_i A_i h_g\rho_g V_g\cdot\boldsymbol{n} \tag{11}$$

Here ε is the porosity, ρ_g is the pyrolysis gas density, V_g is the (superficial) pyrolysis gas velocity, $h_g - h_s$ is the enthalpy of charring, A_i are the areas of the faces of a general finite volume control volume V, and $\boldsymbol{n}$ is the outward unit normal vector for each face. The gas properties, h_g and ρ_g, are functions of temperature and pressure. The solid properties, h_s and k_s, are functions of temperature and density. Mixing rules[37,42] relate the properties for a partially charred solid to the properties of the virgin material and of the char.

The pyrolysis gas flow distribution within the porous solid must also be determined. To make the analysis more tractable, the pyrolysis gas is usually assumed to flow only in the surface-normal direction. Letting x and $\dot{m}_g$ denote a local coordinate pointing inward from the surface and the outward pyrolysis-gas mass flux, respectively, the last term in Eq. (11) becomes

$$+V\frac{\partial}{\partial x}(h_g\dot{m}_g)$$

Furthermore, if the virgin material is nonporous, the gas can only flow outward. In this case, for quasisteady flow, $\dot{m}_g$ can be obtained by integrating the equation

$$\frac{1}{A_x}\frac{\partial(\dot{m}_g A_x)}{\partial x} = \frac{\partial\rho_s}{\partial t} \tag{12}$$

Alternatively, if the virgin material is porous, or if the internal pressure distribution is a concern, it is necessary to solve a transport equation to determine the pressure and flow rate for the pyrolysis gas.[43,44] Mass and momentum conservation equations for one-dimensional pyrolysis gas flow can be written

$$\frac{\partial}{\partial t}[\rho_s + \varepsilon\rho_g] = \frac{\partial\dot{m}_g}{\partial x} \tag{13}$$

$$\frac{\partial\dot{m}_g}{\partial t} = \frac{1}{A_x}\frac{\partial}{\partial x}\left(A_x\frac{\dot{m}_g^2}{\varepsilon\rho_g} + \varepsilon A_x P\right) - c_1\frac{\mu_g\dot{m}_g(1-\varepsilon)^2}{\rho_g\varepsilon^2} - c_2\frac{\dot{m}_g^2(1-\varepsilon)}{\varepsilon^2\rho_g} \tag{14}$$

where c_1 and c_2 are drag coefficients for gas flow through a porous matrix. Under intense heating conditions (e.g., laser heating) internal pressure gradients can lead to mechanical failure (spall) of the char.

Pyrolysis gas flux terms appear in all the surface boundary conditions. Equations (5a), (5b), (6), and (9) become

$$\rho D\frac{\partial\tilde{y}_k}{\partial\eta} = (\dot{m}_{cw} + \dot{m}_{gw})\tilde{y}_k - \dot{m}_{cw}\tilde{y}_{cwk} - \dot{m}_{gw}\tilde{y}_{gwk} \qquad k = 1, N_{\text{el}} \tag{15a}$$

$$\rho D\frac{\partial y_i}{\partial\eta} = \sum_{k=1}^{N_r}\nu_{ki}r_k M_i + (\dot{m}_{cw} + \dot{m}_{gw})y_i - \dot{m}_{cw}Y_{cwi} - \dot{m}_{gw}Y_{gwi} \qquad i = 1, N_c \tag{15b}$$

$$q_w^{\text{CFD}} = (1 - \alpha_{sw})q_r + F\sigma\epsilon_{sw}T_w^4 + q_{\text{cond}} - \dot{m}_{cw}h_{cw} - \dot{m}_{gw}h_{gw} + (\dot{m}_{cw} + \dot{m}_{gw})h_w \tag{16}$$

$$q_{\text{cond}}^{\text{SSEB}} = \dot{m}_{cw}h_{cw} + \dot{m}_{gw}h_{gw} + \dot{m}_{fw}h_{fw} - [\dot{m}_{cw} + \dot{m}_{gw} + \dot{m}_{fw}](h_s)_{\text{in depth}} \tag{17}$$

where the subscripts c and g denote char and pyrolysis gas, respectively. For the transfer coefficient methodology, Eqs. (7) and (8) are unchanged, except that B'_s is replaced by $B'_c + B'_g$.

In limited circumstances, simple $\dot{s}$-T_w and Q^* models are applicable to charring materials. However, in most cases, the surface thermochemistry for charring materials is successfully modeled by thermochemical tables generated by the ACE and GNAT codes using the same methodologies described in Sec. II.B. Specification of the elemental composition of the char, the pyrolysis gas, and the atmosphere allows determination of thermochemical tables similar to those for noncharring materials, except that the dimensionless pyrolysis-gas mass flux becomes an additional independent variable; i.e., the ablation function becomes $\mathcal{F}(T, P, B'_c, B'_g, B'_f) = 0$. Pure thermochemical, kinetic limited, and fail models are applicable for different materials and atmospheres.

Thermochemical B'_c curves for silica phenolic are presented in Fig. 4 at a single pressure and parameterized by B'_g. This case exhibits more complex behavior than seen in the preceding figures, because the char and pyrolysis gas have dissimilar compositions. The major surface species changes from carbon to silica, depending on T_w and B'_g. At small values of B'_g, a silica melt layer exists on the surface. This melt is assumed to flow (fail) at 2000 K in the model shown.

D. CFD Methods for Ablating and Charring Systems

Section II.A. listed CFD issues of importance for nonablating TPS systems. The same concerns apply for ablating and charring systems, except that the pressure is often high enough to warrant the use of a single-temperature model. Surface catalysis is not an issue, but other surface reactions can occur, such as oxidation reactions. Additional concerns are the ablation model, the mass injection of nonair species, the large increase in the number of possible chemical reactions, and the occurrence of nonanalytic, three-dimensional vehicle shapes. Furthermore, for high heating conditions where ablation occurs, radiation can become the dominant heat-transfer mechanism.

Hypersonic flowfields with ablation have been computed by boundary layer, viscous shock layer, PNS, and NS codes. BLIMPK[45,46] is a widely-used CFD code for axisymmetric ablating boundary layers. BLIMPK uses Bartlett's[23] multispecies transport properties and chemical equilibrium or limited kinetic chemistry, both in the gas phase and at the surface. The code does not contain a flowfield radiation model, but it allows a prescribed radiative flux q_r. BLIMPK can be run with an SSEB [Eqs. (16) and (17)] to determine as part of the solution the surface temperature and the surface mass fluxes $\dot{m}_{cw}$ and $\dot{m}_{gw}$. There is no need to input thermochemical ablation tables, because ACE is essentially contained within the BLIMPK code.

Three codes (COLTS,[47] HYVIS,[48] and RASLE[49]) were developed as part of Project Galileo for the analysis of axisymmetric, strongly radiating viscous shock layers. These codes differ in the transport properties, CFD numerics, and in the extent of coupling between fluid dynamics and radiation transport, but all three use multiband, gray-gas radiation models.[50-52] RASLE can solve the SSEB [Eqs. (6) and (9)] to compute the ablation flux $\dot{m}_{sw}$ and wall temperature. Gupta et al.[53] used a similar approach to solve an Earth re-entry problem.

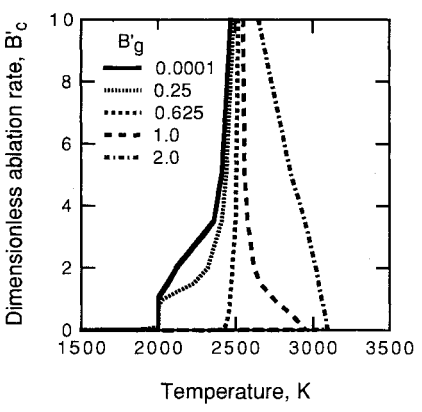

Fig. 4 Dimensionless ablation rate for silica phenolic. Thermochemical solution with partial fail at 2000 K; P = 1 atm.

Recently, there has been a renewed interest in the computation of ablative flowfields with chemical reactions. Conti et al.[54] computed an axisymmetric NS solution with pure carbon ablation, shape change, and variable surface temperature, but with no chemistry and an incomplete SEB. Bhutta and Lewis[55] computed a slightly three-dimensional PNS flowfield with Teflon® ablation. The solution included kinetic Teflon-air chemistry and a steady-state ablation model at constant wall temperature. Neither of these solutions considered radiation transport.

Although considerable uncertainties remain in multispecies transport coefficients and chemical kinetics models, the plethora of gas-phase species in ablative flowfields is no longer the major stumbling block for CFD computations, at least in two dimensions. The current state-of-the-art for PNS and NS calculations appears to be full gas-phase kinetics and simplified ablation modeling. References 55–57 contain data bases of chemical reactions and reaction coefficients for CFD calculation of ablative flowfields in thermal equilibrium.

The next step forward for PNS and NS calculations is to allow a variable surface temperature to be determined as part of a solution that also contains more sophisticated ablation models and a coupled SSEB. It should be noted, however, that use of the SSEB at low ablation rates can result in overestimated values for the surface temperatures and the ablation rate. For trajectory-based or other transient analyses where thermal soak is important, CFD methods should be coupled with a numerical or semianalytic CSM method that can predict q_{cond} at every surface point. This topic is discussed further in Sec. III.A.

No CFD code currently handles the general case of thermochemical ablation with or without surface reactions. Shape change is also a problem, because most CFD codes cannot robustly handle arbitrary nonanalytic shapes, particularly in three dimensions.

Radiation transport in ablating flowfields is an extremely difficult computational problem. A new generation of multiband, gray-gas radiation models has been developed,[58,59] but these models are not yet applicable to ablating flowfields owing to the lack of a complete data base of model parameters for ablation-product species. Alternatives to the one-dimensional tangent-slab approximation for radiation transport have also been investigated.[60,61]

Ablation-induced turbulence is another concern. Park[62] suggests that ablation can greatly increase the level of turbulent kinetic energy and heat transfer in a boundary-layer flow. This concern has not been thoroughly addressed by the CFD or thermophysics communities.

III. Semianalytic Models

Surface mass and energy balances, a catalysis model, and an ablation model provide the surface thermochemical boundary conditions that should be used for a realistic, multidisciplinary CFD-CSM solution of the flow past a hypersonic vehicle. Unfortunately, no single code or set of codes currently exists which can solve simultaneously the fully-coupled CFD-CSM problem. However, in many circumstances, good design solutions can be obtained by using a detailed numerical model for one-half of the problem, an approximate semianalytic method for the other half, and the surface energy balance and ablation model as boundary conditions. This section highlights certain semianalytic CSM and CFD models that can be used for this purpose.

A. Approximate CSM Solutions

Transient heat conduction obviously affects the surface temperature and recession history of an aerodynamically heated TPS material. A solution of the in-depth heat-conduction

equation with proper surface boundary conditions and a suitable ablation model is required for a precise calculation. However, an approximate solution can be obtained efficiently by using an integral method in lieu of a detailed heat-conduction solution.

The heat-balance integral (HBI) method was developed by Goodman[63,64] and extended by many researchers to include the effects of variable properties and surface ablation. The analysis begins with the equation for one-dimensional heat conduction in a solid. In terms of a coordinate z that moves with the receding surface, the one-dimensional heat conduction equation becomes

$$\rho c_p \frac{\partial T}{\partial t} = \frac{\partial}{\partial z}\left(k \frac{\partial T}{\partial z}\right) + \rho c_p \dot{s} \frac{\partial T}{\partial z} \tag{18}$$

$\dot{s}$ is an unknown function of time. The thermal conductivity, specific heat, and solid density may be functions of temperature. The boundary conditions are

$$T = T_{\text{init}} \quad \text{at} \quad t = 0$$

$$k \frac{\partial T}{\partial z} = -q_{\text{cond}} \quad \text{at} \quad z = 0$$

$$\frac{\partial T}{\partial z} = 0 \quad \text{at} \quad z = \delta_T$$

where δ_T is a representative thermal-layer thickness.

The two key steps of the analysis are to transform the dependent variable

$$\xi = \int_{T_{\text{init}}}^{T} \rho c_p \, dT \tag{19}$$

and to assume a shape for the transformed temperature profile

$$\xi = \xi_w[1 - (z/\delta_T)]^b \tag{20}$$

The constant b is set at 3 for consistency with the boundary conditions. Higher-order profiles can also be used.[64] Substitution of the above expressions into Eq. (18), integration from $z = 0$ to $z = \delta_T$, integration over time, and application of the boundary conditions yields

$$\xi_w = \left[\frac{(b+1)q_{\text{cond}}}{b}\left(\frac{\rho c_p}{k}\right)_w \int_0^t (q_{\text{cond}} - \dot{s}\xi_w)\, dt\right]^{1/2} \tag{21}$$

The heat balance integral, Eq. (21), provides a relationship between the conduction heat flux to the surface q_{cond}, the recession rate $\dot{s}$, and the transformed surface temperature ξ_w. The surface energy balance [Eq. (6)] and the ablation model (cf. Sec. II) are additional relationships between q_{cond}, $\dot{s}$, and T_w. Therefore, the HBI, coupled with the surface energy balance and a suitable ablation model, provides a complete set of time-dependent thermal boundary conditions for the CFD solution of the flow past ablating or nonablating surfaces.

By combining the HBI with the SEB, the transient heat conduction into the TPS material can be taken into account, and realistic estimates can be made for the time- and location-dependent aerothermal heat loads on the thermal protection system. However, the procedure can be computationally expensive, because steady CFD calculations must be performed at sequence of times along the trajectory starting from an initial condition. For the ablating case, mass injection of ablating species and recession of the surface into a nonanalytic shape are complications for the CFD analysis. An example of the HBI method fully coupled with the SEB, a thermochemical ablation model, and shape change is described in Sec. III.C.

The HBI is a one-dimensional approximation and, therefore, cannot simulate multidimensional conduction effects. The HBI can become inaccurate for vehicles with very small nose radius and for long duration or cyclical heating environments.

The HBI method is not directly applicable to charring TPS materials. For this case, Potts[65] recommends a hybrid HBI/quasisteady solution. In this procedure a two-layer model for the energy equation is combined with a quasisteady assumption for certain terms such that the pyrolysis gas flux $\dot{m}_{gw}$ can be obtained as part of the solution.

B. Approximate CFD Solutions

Thermal protection systems are designed and optimized by performing transient analyses of the thermophysics of aerodynamically heated materials. A transient CSM solution with thermophysics can, in principal, be computed by using as boundary conditions a suitable ablation model and the SEB [Eqs. (6) or (16)] with aerothermal heating q_w^{CFD} prescribed as a function of location and time. However, there is no straightforward CFD method for computing the aerothermal heat flux, because q_w^{CFD} is a strong function of the unknown blowing rate. This coupling cannot be circumvented. Therefore, efforts have focused on the development of robust, approximate CFD methods which can be solved concurrently with the coupled, transient CSM solution.

The most successful approach to date is the momentum/energy integral technique (MEIT),[66] which solves the integral boundary-layer equations for heat and mass transfer. We briefly follow here the derivation of Ref. 66, which should be consulted for further details. The analysis begins with basic definitions of the boundary-layer thickness parameters

$$\delta^* = \int_0^\infty \left(1 - \frac{\rho u}{\rho_i u_i}\right) dy \qquad \theta = \int_0^\infty \frac{\rho u}{\rho_e u_e}\left(\frac{u_i - u}{u_e}\right) dy$$

$$\phi = \int_0^\infty \frac{\rho u}{\rho_e u_e}\left(\frac{h_i^t - h^t}{h_e^t - h_w}\right) dy \qquad \delta_e^* = \int_0^\delta \left(1 - \frac{\rho u}{\rho_e u_e}\right) dy$$

and the shape and recovery factors

$$\mathcal{G} = \frac{(\delta - \delta_e^*)}{\theta} \qquad \mathcal{H} = \frac{\delta^*}{\theta} \qquad \mathcal{R} = \frac{h_r - h_e}{h_e^t - h_e}$$

where the subscripts e and i denote, respectively, the edge and normal shock-edge values.

In terms of these quantities, the axisymmetric boundary-layer integral momentum and energy equations become

$$\frac{1}{r_b \rho_e u_e^2} \frac{d}{ds}[r_b \rho_e u_e^2 \theta] = \frac{C_f}{2} + \frac{\dot{m}_{sw} u_{iw}}{\rho_e u_e^2} + \frac{\mathcal{H}\theta}{\rho_e u_e^2} \frac{dp}{ds} \tag{22}$$

$$\frac{1}{r_b \rho_e u_e (h_e^t - h_w)} \frac{d}{ds}[r_b \rho_e u_e (h_e^t - h_w)\phi]$$

$$= \frac{C_h(h_r - h_w)}{h_e^t - h_w} + \frac{\dot{m}_{sw}(h_{iw}^t - h_w)}{\rho_e u_e (h_e^t - h_w)} \tag{23}$$

where s is a streamlength coordinate.

One additional equation, an entrainment relation, links the boundary-layer mass flux to a specific shock location

$$\rho_\infty u_\infty r_{\text{shock}}^2 = 2 r_b \mathcal{G} \mu_e Re_\theta - 2 \int_0^s r_b \dot{m}_{sw} \, ds \tag{24}$$

This equation enables the calculation of thermodynamic properties at the boundary-layer edge from a known shock shape.

For laminar or turbulent hypersonic flow over a flat plate, the unblown Stanton number C_{h0}, unblown skin friction coefficient $C_{f0}/2$, and the factors $\mathcal{G}$, $\mathcal{H}$, and $\mathcal{R}$ are all prescribed

functions of the wall and edge conditions, the Prandtl number, and the Reynolds numbers Re_θ and Re_ϕ. To compute the solution for any general shape and flow conditions, $\mathcal{G}$, $\mathcal{H}$, and $\mathcal{R}$ are not corrected, but C_h and C_f are defined as the unblown values times the product of all known influence coefficients

$$C_h = C_{h0} \prod^{l} I_l \qquad C_f = C_{f0} \prod^{l} J_l$$

where the subscript l designates the effects of acceleration, blowing, variable properties, transition proximity, and other phenomena. The influence coefficients I_l and J_l are derived from exact solutions, theories, CFD numerical solutions, and data. For example, the influence coefficient for blowing, from Eq. (8), is

$$I_{B'} = \frac{2\lambda B'}{e^{2\lambda B'} - 1}$$

The analysis hinges on obtaining an accurate estimate of the surface pressure for the inviscid flow. The pressure distribution may be obtained from inviscid CFD solutions or from correlations.[10,66] An approximate shock shape can be obtained using the surface pressure and global mass and momentum balances. With this inviscid-flow information, the solution of Eqs. (22) and (23) for θ, ϕ, and all the other quantities, can be marched forward starting from the stagnation point. The MEIT solution is coupled with the SEB [Eqs. (6) and (7)], the thermochemical ablation tables which provide the blowing rate B', and a transient CSM solver which provides q_{cond} and T_w.

In three dimensions, the inviscid-flow procedures are not as straightforward. The MASCC code[12] uses an axisymmetric approximation to predict the flowfield. In this procedure, an effective body radius is determined by rotating the body into a wind-fixed coordinate system. The surface pressure and shock shape are then obtained by the axisymmetric procedures described above. Finally, the MEIT calculations are performed for a set of surface streamlines starting from the stagnation point. The streamlines are calculated by a method of steepest descent based on the body shape and the inviscid flow information. The ablation at any point on the surface is obtained by interpolation of the streamline solutions.

C. CST Example

This section presents an illustrative example of TPS analysis using CST boundary conditions and the semianalytic methods described in preceding sections. The example problem is a hypersonic test vehicle with a small initial nose radius (1.75 cm) and graphite TPS which travels near Mach 16 at an altitude of 30.5 km. The problem is axisymmetric. The calculations are performed by the ablation shape change (ASC) code[10] which utilizes the semianalytic boundary-layer and inviscid flow procedures described in Sec. III.B.

The NASA Ames version of ASC contains four options for calculation of the conduction heat flux term q_{cond} in the SEB. In order of decreasing accuracy, the boundary condition options are 1) detailed transient heat conduction analysis; 2) HBI method to approximate the transient heat conduction; 3) SSEB method which uses the quasisteady value; and 4) REEB method which sets $q_{cond} = 0$.

The primary option to obtain q_{cond} is a finite difference, heat conduction solution which determines the transient temperature distribution throughout the interior of the vehicle. The ASC solution follows a trajectory starting from an initial condition of prescribed altitude and temperature below the value required for ablation. Therefore, the initial flowfield is unblown. In general, a large number of conduction time steps may be computed for every steady flowfield solution. However, the steady inviscid flow and blown or unblown boundary-layer solutions are recalculated whenever the surface temperature, heat flux, vehicle shape, vehicle velocity or altitude have changed by a significant amount. The solid and fluid dynamics solutions are coupled through the SEB and thermochemical ablation model.

For option 2, the heat conduction solver is replaced by the HBI integral, Eq. (21), which provides a one-dimensional approximation for the transient thermal energy stored in the vehicle. The solution is marched along the trajectory in the same manner, but with larger time steps than for option 1. The SSEB and REEB options disregard transient heating effects.

For all four boundary condition options, both shape-change and no-shape-change ASC calculations were made. The latter case is used only to compare results without the additional complication of differences in vehicle shape. The surface temperature history for the four no-shape-change runs is presented in Fig. 5. The SSEB and REEB solutions are independent of time at constant shape, altitude, and velocity. The REEB surface temperature exceeds the SSEB surface temperature everywhere and varies from about 100 K higher on the spherical portion of the vehicle to 10 K higher at the base.

For the time-dependent options, the initial temperature was chosen to be 500 K. As shown in Fig. 5, the stagnation point region heats up rapidly. Nevertheless, after 60 s of heating the transient temperature remains over 100 K below the SSEB value and over 200 K below the REEB value at the stagnation point. The REEB and SSEB solutions are highly unrealistic for the conical portion of the vehicle, where after 60 s of heating the errors range from 500–800 K. The HBI solution provides a good approximation to the transient heat-conduction along the forward portion of the vehicle, but underpredicts the temperature on the slowly heated frustrum.

To compare ablation predictions for the four options, the ASC runs were repeated with shape change turned on. The initial shape and the shapes after 15 and 30 s are shown in Fig. 6. The three approximate models are reliable close to the stagnation point, but only the HBI method provides any accuracy elsewhere on the vehicle. The SSEB and REEB predictions are particularly erroneous on the shoulder of the vehicle and along the conical frustrum. The REEB is worse than the SSEB everywhere, but not by a large amount in this example. The errors in the mass loss predictions are under 9% for the HBI method and over 220% for both the SSEB and REEB options.

Clearly, the SSEB and REEB boundary conditions should be used with caution. These approximations can estimate the surface temperature at high heating conditions near the stagnation point. However, away from the stagnation point a long heating duration may be required for the surface temperature to approach the SSEB or REEB values. For a slender ablating vehicle, the shape can change significantly in this length of

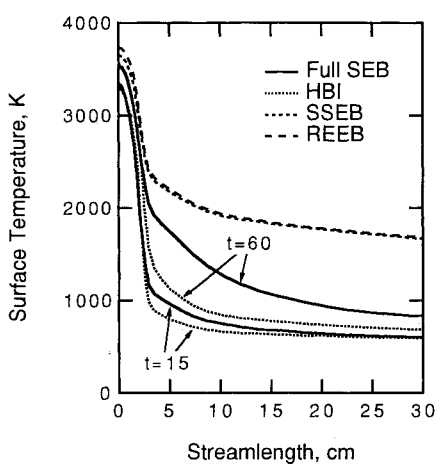

Fig. 5 Surface temperature for ASC example problem with no shape change and four boundary condition options.

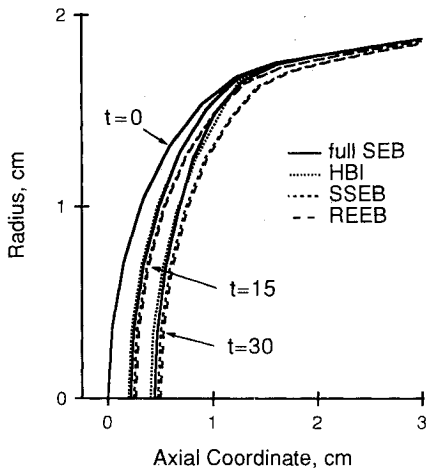

Fig. 6 Initial shape and ablated shapes at two times for ASC example problem with four boundary condition options.

time, but these two methods are not reliable for predicting the shape change in this case.

This axisymmetric example was not computationally expensive. The longest run, shape change with detailed transient heat conduction, required about 20 min to compute on a Sun SPARC station 2. The SSEB and REEB options took about 2 min. The HBI option, which required iteration between the SEB and HBI equations, took 8 min. For a three-dimensional problem, the HBI method would be at least an order of magnitude faster than a transient heat conduction solution. The most cost-effective procedure is option 2 which couples CST boundary conditions with semianalytic approximations for both the CFD and CSM portions of the problem.

It should be noted that the trends in the above results are typical and not highly specific to the particular geometry and flow conditions of this example. Further details on the capabilities and limitations of multi-dimensional CST procedures will be documented in a future publication.

IV. Discussion

Computational expense currently prohibits the simultaneous use of detailed CFD and CSM procedures for solution of the fully-coupled transient analysis of TPS response for a hypersonic vehicle. In fact, codes are not available which contain all the necessary thermophysics in either the solid or the fluid regions. Both CFD and CSM codes must be improved to solve in two and three dimensions all the near-surface thermophysics described in Sec. II. Full CST boundary conditions should be coupled with the semianalytic methods as discussed in Sec. III.

For the CFD/CST problem, solutions for the nonablating case have been obtained by Chen et al.[16] with all the important thermophysics except for the heat conduction term in the surface energy balance. This term can be obtained by coupling the HBI method with the SEB to create a CFD code capable of performing true trajectory-based aerothermal heating predictions in two dimensions. However, it remains to be seen whether or not such a code could practically be run at many times or altitudes along a trajectory.

A procedure needs to be developed for coupling the SEB with thermochemical ablation tables. These tables, generated using the ACE or GNAT codes, relate the ablation rate to the mass transfer coefficient and to the surface temperature and pressure. Species concentrations of the gaseous ablation products at the surface are also computed as part of the solution, but generally are not saved for later use. The most direct way to incorporate these B' tables into a CFD code may be to save the ablation mass ratios Y_{swi} for the major species which appear in the CFD surface mass balance, Eqs. (5b) or (15b). The CFD surface energy balance, Eqs. (6) or (16), will correctly account for the heat of ablation. The mass-transfer coefficient $\rho_e u_e C_m$ must be obtained from the CFD solution to dimensionalize B'.

Conclusions

The models, equations, and numerical solution techniques for surface thermochemistry and near-surface thermophysics have been reviewed and discussed. Particular emphasis has been placed on appropriate forms of the surface mass and energy balances for the cases of surface catalysis, ablation, and ablation with pyrolysis.

The surface balances, combined with suitable ablation and catalysis models, provide complete CST boundary conditions for the multidisciplinary numerical solution of the coupled CFD/CSM problem for TPS analysis. Approximate semianalytic methods exist which can be coupled with CST boundary conditions so that realistic, practical solutions can be obtained for either the CFD or CSM portions of the problem.

All the basic models and equations for TPS material thermophysics have been presented herein. These equations need to be incorporated into new or existing multidimensional CSM codes. A significant increase in the state-of-the-art in aerothermal CFD technology is possible by uniting CFD methodology with CST boundary conditions and the HBI method.

Acknowledgments

The authors greatly appreciate the input from conversations with Y.-K. Chen, W. D. Henline, T. H. Squire, and D. A. Stewart at the NASA Ames Research Center and R. A. S. Beck and C. L. Minell from the Aerotherm Corporation.

References

[1]Anon., *Mars Environmental Survey (MESUR) Science Objectives and Mission Description*, MESUR Study Office Rept., NASA Ames Research Center, July 19, 1991.

[2]Kendall, R. M., Bartlett, E. P., Rindal, R. A., and Moyer, C. B., "An Analysis of the Chemically Reacting Boundary Layer and Charring Ablator. Part I: Summary Report," NASA CR-1060, June 1968.

[3]Moyer, C. B., and Rindal, R. A., "An Analysis of the Chemically Reacting Boundary Layer and Charring Ablator. Part II: Finite Difference Solutions for the In-Depth Response of Charring Materials Considering Surface Chemical and Energy Balances," NASA CR-1061, June 1968.

[4]Bartlett, E. P., and Kendall, R. M., "An Analysis of the Chemically Reacting Boundary Layer and Charring Ablator. Part III: Nonsimilar Solution of the Multicomponent Laminar Boundary Layer by an Integral Matrix Method," NASA CR-1062, June 1968.

[5]Anon., "User's Manual Aerotherm Chemical Equilibrium Computer Program (ACE 81)," Acurex Corp., Rept. UM-81-11/ATD, Mountain View, CA, Aug. 1981.

[6]Kelly, J. T., "User's Manual, General Nonequilibrium Ablation Thermochemistry (GNAT) Computer Program," Acurex Corp., Rept. UM-74-57, Mountain View, CA, Oct. 1974.

[7]Risch, T. K., and Laub, B., "General Model for Thermochemical Ablation into a Vacuum," *Journal of Thermophysics and Heat Transfer*, Vol. 4, No. 3, 1990, pp. 278–284.

[8]Laub, B., Suchland, K. E., and Murray, A. L., "Mathematical Modeling of Ablation Problems," *Computational Techniques for Interface Problems*, edited by K. C. Park, and D. K. Gartling, Vol. 30, Applied Mechanics Div. Ser., American Society of Mechanical Engineers, New York, 1978, pp. 97–115.

[9]Kendall, R. M., and Anderson, L. W., "Nonsimilar Solutions for Laminar and Turbulent Boundary-Layer Flows over Ablating Surfaces," *AIAA Journal*, Vol. 10, No. 9, 1972, pp. 1230–1236.

[10]Rafinejad, D., Dahm, T. J., Brink, D. F., Abbett, M. J., and Wolf, C. J., "Passive Nosetip Technology (PANT II) Program, Volume 2. Computer User's Manual: ABRES Shape Change Code (ASCC)," Acurex Corp., Rept. SAMSO-TR-77-11, Mountain View, CA, Oct. 1976.

[11]King, H. H. C., Muramoto, K. K., Murray, A. L., and Pronchick, S. W., "ABRES Shape Change Code (ASCC 86): Technical Report and User's Manual," Acurex Corp., Rept. FR-88-24/ATD, Mountain View, CA, Dec. 1986.

[12]Squire, T. H., and Murray, A. L., "Maneuvering ABRES Shape Change Code (MASCC88). Technical Report and User's Manual,"

Acurex Corp., Rept. FR-88-15/ATD, Mountain View, CA, Sept. 1988.

[13]Kolodziej, P., and Stewart, D. A., "Nitrogen Recombination on High Temperature Reusable Surface Insulations and the Analysis of Its Effect on Surface Catalysis," AIAA Paper 87-1637, June 1987.

[14]Stewart, D. A., and Kolodziej, P., "Wall Catalysis Experiments on AFE," AIAA Paper 88-2674, June 1988.

[15]Stewart, D. A., Chen, Y.-K., and Henline, W. D., "Effect of Non-Equilibrium Flow Chemistry and Surface Catalysis on Surface Heating to AFE," AIAA Paper 91-1373, June 1991.

[16]Chen, Y.-K., Henline, W. D., Stewart, D. A., and Candler, G. V., "Navier-Stokes Solutions with Surface Catalysis for Martian Atmospheric Entry," AIAA Paper 92-2946, July 1992.

[17]Lashkari, M., "COSMOS/M User Guide, Volume 1," Structural Research and Analysis Corp., Santa Monica, CA, April 1992.

[18]Bhutta, B. A., and Lewis, C. H., "Prediction of Supersonic/Hypersonic Flows over Re-Entry Vehicles and Decoys," *Journal of Spacecraft and Rockets*, Vol. 27, No. 5, 1990, pp. 493–502.

[19]Bhutta, B. A., and Lewis, C. H., "Prediction of Three-Dimensional Hypersonic Flows Using a Parabolized Navier-Stokes Scheme," *Journal of Spacecraft and Rockets*, Vol. 26, No. 1, 1989, pp. 4–13.

[20]Bhutta, B. A., and Lewis, C. H., "Comparison of Hypersonic Experiments and PNS Predictions. Part I: Aerothermodynamics," *Journal of Spacecraft and Rockets*, Vol. 28, No. 4, 1991, pp. 376–386.

[21]Gnoffo, P. A., Gupta, R. N., and Shinn, J. L., "Conservation Equations and Physical Models for Hypersonic Air Flows in Thermal and Chemical Nonequilibrium," NASA TP-2867, Feb. 1989.

[22]Park, C., "Chemical-Kinetic Problems of Future NASA Missions. I. Earth Entries: A Review," *Journal of Thermophysics and Heat Transfer* (submitted for publication); see also AIAA Paper 91-0464, Jan. 1991.

[23]Bartlett, E. P., Kendall, R. M., and Rindal, R. A., "An Analysis of the Chemically Reacting Boundary Layer and Charring Ablator. Part IV: A Unified Approximation for Mixture Transport Properties for Multicomponent Boundary-Layer Applications," NASA CR-1063, June 1968.

[24]Wilke, C. R., "A Viscosity Equation for Gas Mixtures," *Journal of Chemical Physics*, Vol. 18, No. 4, 1950, pp. 517–519.

[25]Blottner, F. G., Johnson, M., and Ellis, M., "Chemically Reacting Viscous Flow Program for Multi-Component Gas Mixtures," Sandia National Lab., Rept. SR-RR-70-754, Albuquerque, NM, Dec. 1971.

[26]Vincenti, W. G., and Kruger, C. H., *Introduction to Physical Gas Dynamics*, Krieger Publishing, Malabar, FL, 1965.

[27]Lee, J. H., "Basic Governing Equations for the Flight Regimes of Aeroassisted Orbital Transfer Vehicles," *Thermal Design of Aeroassisted Orbital Transfer Vehicles*, edited by H. F. Nelson, Vol. 96, Progress in Aeronautics and Astronautics, AIAA, New York, 1985, pp. 3–53.

[28]Tauber, M. E., and Sutton, K., "Stagnation-Point Radiative Heating Relations for Earth and Mars Entries," *Journal of Spacecraft and Rockets*, Vol. 28, No. 1, 1991, pp. 40–42.

[29]Stewart, D. A., Rakich, J. V., and Lanfranco, M. J., "Catalytic Surface Effects on Space Shuttle Thermal Protection System During Earth Entry of Flights STS-2 through STS-5," NASA CP-2283, March 1983.

[30]Perry, R. H., and Chilton, C. H., *Chemical Engineer's Handbook*, 5th ed., McGraw-Hill, New York, 1973.

[31]Wise, H., and Wood, B. J., "Reactive Collisions Between Gas and Surface Atoms," *Advances in Molecular and Atomic Physics*, Vol. 3, Academic Press, New York, 1967, pp. 291–353.

[32]Seward, W. A., and Jumper, E. J., "Model for Oxygen Recombination on Silicon-Dioxide Surfaces," *Journal of Thermophysics and Heat Transfer*, Vol. 5, No. 3, 1991, pp. 284–291.

[33]Jumper, E. J., and Seward, W. A., "Model for Oxygen Recombination on Silicon-Dioxide Surfaces: Part II, Implications Toward Reentry Heating," AIAA Paper 92-0811, Jan. 1992.

[34]Williams, S. D., and Browning, R. E., "Pathfinder Thermophysical Property Data—Thermal Protection Materials for High Energy Aerobraking Vehicles," Vol. 1, Lockheed Engineering and Sciences, Rept. LESC-27438, Houston, TX, Aug. 1989.

[35]Squire, T. H., Kolodziej, P., and Hartlieb, G., private communication, NASA Ames Research Center, April 27, 1992.

[36]Weber, G. A., and Bartle, R. S., "Thermal Design Properties Handbook," Rept. KHDR-AVMSD-68-3, Avco Missiles, Space, and Electronics Group, Missile Systems Div., Wilmington, MA, May 1968.

[37]Anon., "User's Manual Aerotherm Charring Material Thermal Response and Ablation Program CMA87," Acurex Corp., Rept. UM-87-11/ATD, Mountain View, CA, Aug. 1987.

[38]Kendall, R. M., Rindal, R. A., "An Analysis of the Chemically Reacting Boundary Layer and Charring Ablator. Part V: A General Approach to the Thermochemical Solution of Mixed Equilibrium-Nonequilibrium, Homogeneous or Heterogeneous Systems," NASA CR-1064, June 1968.

[39]Scala, S. M., "The Ablation of Graphite in Dissociated Air. I: Theory," General Electric, Missile and Space Div., Rept. R62SD72, Philadelphia, PA, Sept. 1962.

[40]Spalding, D. B., *Convective Mass Transfer*, Edward Arnold Ltd., London, 1963.

[41]Rasky, D. J., private communication, NASA Ames Research Center, April 24, 1992.

[42]Clever, R. M., and Denny, V. E., "Response of Charring Ablators to Severe Aerodynamic and Erosion Environments," *Journal of Spacecraft and Rockets*, Vol. 12, No. 9, 1975, pp. 558–564.

[43]Milos, F. S., Risch, T. K., and Beck, R. A. S., "Numerical Analysis of Thermochemical Response of Hardening Materials to Pulsed Laser Heating," AIAA Paper 89-0177, Jan. 1989.

[44]Popper, L., "Repetitively Pulsed Modeling," Physical Sciences, Rept. PSI-445/TR-594, Andover, MA, Aug. 1986.

[45]Evans, R. M., "User's Manual, Boundary Layer Integral Matrix Procedure Including Gas Phase Kinetics, KBLIMP-A," Acurex Corp., Rept. UM 75-62, Mountain View, CA, March 1975.

[46]Murray, A. L., "Further Enhancements of the BLIMP Computer Code and User's Guide," Acurex Corp., Rept. Air Force Wright Aeronautical Lab. TR-88-3010, Mountain View, CA, June 1988.

[47]Kumar, A., Tiwari, S. N., and Graves, R. A., Jr., "Radiating Viscous Shock Layer Solutions for Jovian Entry at Angle of Attack," *Outer Planet Entry Heating and Thermal Protection*, edited by R. Viskanta, Vol. 64, Progress in Astronautics and Aeronautics, AIAA, New York, 1979, pp. 147–164.

[48]Moss, J. N., Anderson, E. C., and Bolz, C. W., Jr., "Aerothermal Environment for Jupiter Entry Probes," *Thermophysics of Spacecraft and Outer Planet Entry Probes*, edited by A. M. Smith, Vol. 56, Progress in Astronautics and Aeronautics, AIAA, New York, 1976, pp. 333–354.

[49]Nicolet, W. E., Waterland, L. R., and Kendall, R. M., "Methods for Predicting Radiation-Coupled Flowfields About Planetary Entry Probes," *Aerodynamic Heating and Thermal Protection Systems*, edited by L. S. Fletcher, Vol. 59, Progress in Astronautics and Aeronautics, AIAA, New York, 1978, pp. 120–136.

[50]Nicolet, W. E., "Rapid Methods for Calculating Radiation Transport in the Entry Environments," NASA CR-2528, April 1975.

[51]Nicolet, W. E., "User's Manual for the Generalized Radiation Transfer Code (RAD/EQUIL)," NASA CR-116353, Oct. 1969.

[52]Zoby, E. V., Sutton, K., Olstad, W. B., and Moss, J. N., "Approximate Inviscid Radiating Flowfield Analysis for Outer Planet Entry Probes," *Outer Planet Entry Heating and Thermal Protection*, edited by R. Viskanta, Vol. 64, Progress in Astronautics and Aeronautics, AIAA, New York, 1979, pp. 42–64.

[53]Gupta, R. N., Lee, K.-P., Moss, J. N., and Sutton, K., "Viscous-Shock-Layer Solutions with Coupled Radiation and Ablation Injection for Earth Entry," *Journal of Spacecraft and Rockets*, Vol. 29, No. 2, 1992, pp. 173–181.

[54]Conti, R. J., MacCormack, R. W., Groener, L. S., and Fryer, J. M., "Practical Navier-Stokes Computation of Axisymmetric Reentry Flowfields with Coupled Ablation and Shape Change," AIAA Paper 92-0752, Jan. 1992.

[55]Bhutta, B. A., and Lewis, C. H., "Low-to-High Altitude Predictions of Three-Dimensional Ablative Reentry Flowfields," AIAA Paper 92-0366, Jan. 1992.

[56]Finson, M. L., Ameer, P. G., Person, J. C., Cronin, J. F., and Parker, P. D., "Non-Equilibrium Boundary Layer Code, Volume I—Numerical Methodology," Physical Sciences, Rept. BMO-TR-88-27, Andover, MA, June 1988.

[57]Baulch, D. L., Cox, R. A., Crutzen, P. J., Hampton, R. F., Jr., Kerr, J. A., Troe, J., and Watson, R. T., "Evaluated Kinetic and Photochemical Data for Atmospheric Chemistry: Supplement 1," *Journal of Physical Chemistry Reference Data*, Vol. 11, No. 2, 1982, pp. 326–497.

[58]Hartung, L. C., "Development of a Nonequilibrium Radiative Heating Prediction Method for Coupled Flowfield Solutions," AIAA Paper 91-1406, June 1991.

[59]Park, C., "Calculation of Nonequilibrium Radiation in the Flight Regimes of Aeroassisted Orbital Transfer Vehicles," *Thermal Design of Aeroassisted Orbital Transfer Vehicles*, edited by H. F. Nelson, Vol. 96, Progress in Aeronautics and Astronautics, AIAA, New York, 1985, pp. 395–418.

[60]Hartung, L. C., and Hassan, H. A., "Radiation Transport Around

Axisymmetric Blunt Body Vehicles Using a Modified Differential Approximation," AIAA Paper 92-0119, Jan. 1992.

[61]Cinnella, P., and Elbert, G. J., "Two-Dimensional Radiative Heat Transfer Calculations for Flows in Thermo-Chemical Non-Equilibrium," AIAA Paper 92-0121, Jan. 1992.

[62]Park, C., "Injection-Induced Turbulence in Stagnation-Point Boundary Layers," *AIAA Journal*, Vol. 22, No. 2, 1984, pp. 219–225.

[63]Goodman, T. R., "The Heat-Balance Integral and Its Application to Problems Involving a Change of Phase," *Transactions of the American Society of Mechanical Engineers*, Vol. 80, No. 2, 1958, pp. 335–342.

[64]Goodman, T. R., "The Heat-Balance Integral—Further Considerations and Refinements," *Journal of Heat Transfer*, Vol. 83, No. 1, 1961, pp. 83–86.

[65]Potts, R. L., "Hybrid Integral/Quasi-Steady Solution of Charring Ablation," AIAA Paper 90-1677, June 1990.

[66]Dahm, T. J., Cooper, L., Rafinejad, D., Youngblood, S. B., and Kelly, J. T., "Passive Nosetip Technology (PANT II) Program, Volume 1. Inviscid Flow and Heat Transfer Modeling for Reentry Vehicle Nosetips," Acurex Corp., Rept. SAMSO-TR-77-11, Mountain View, CA, Oct. 1976.